Theoretical and Applied Fracture Mechanics 116 (2021) 103122

Contents lists available at ScienceDirect

Theoretical and Applied Fracture Mechanics

journal homepage: www.elsevier.com/locate/tafmec

Mixed mode equilibrium analysis of asymptotic fields around stationary sharp V-notches in polymer gels: A linear poroelastic study

Yunlong Li [a,*], Zheng Niu [a], Xianjia Chen [b,*]

[a] Institute of Solid Mechanics, School of Aeronautic Science and Engineering, Beihang University, Beijing 100191, China
[b] The State Key Laboratory of Nonlinear Mechanics, Institute of Mechanics, Chinese Academy of Sciences, Beijing 100190, China

ARTICLE INFO

Keywords:
Mixed mode loadings
Asymptotic solution
Sharp V-notches
Thermodynamic equilibrium
Poroelasticity
Polymer gels

ABSTRACT

In this paper, the equilibrium asymptotic stress and solvent concentration fields around stationary sharp V-notches are extracted for in-plane mixed mode loadings employing the linear poroelasticity theory. It is shown that at thermodynamic equilibrium, mechanical and chemical equilibrium equations are uncoupled and thus can be solved independently. The mechanical equilibrium equations are then solved using the Airy stress function technique. This technique replaces the coupled mechanical equilibrium relations with the compatibility biharmonic equation which can be solved using the separation of variables method. Applying traction free boundary conditions on the notch edges leads to an eigenvalue problem which gives both mode I and mode II eigenvalues. These eigenvalues can be real or complex numbers depending on the notch opening angle. Since there are infinite eigenvalues for both modes of deformation, series solutions will be obtained for the equilibrium fields. From these asymptotic solutions, it is found that the obtained stress fields are similar to their corresponding linear elasticity solution. Furthermore, from the solutions, it can be observed that the opening and shear deformations near the notch tip lead to cosine and sine variations of the solvent concentration field with respect to the angular coordinates, respectively. The accuracy of these asymptotic results is finally verified using finite element analyses of a single-edge notched (SEN) specimen subjected to far field applied small displacements. The numerical analyses are performed for two notch opening angles of 30° and 60° for both plane stress and plane strain conditions. The comparative study between the finite element results and the asymptotic solution proves that the present solution can accurately capture the near notch tip stress and solvent concentration fields by considering only the first few terms of the series solutions.

1. Introduction

Polymer gels are essentially biphasic materials composed of an elastic polymer network swollen by a solvent (e.g. water) as the second phase. These soft materials possess exceptional mechanical and chemical properties which make them ideal candidates for a diverse range of applications including soft actuators [1], drug delivery systems [2], microvalves [3] and tissue engineering [4]. In many of these applications, gels are subjected to mechanical loads and displacements and thus their failure assessment is essential. On the other hand, stress concentrators like cracks and sharp corners are frequently seen in these soft structures due to their versatile geometries. Lee and Jho [5], for instance, utilized a V-notched hydrogel structure as a temperature sensitive bilayer gripper which is able to lift and release objects much heavier than the gripper itself. Similar notched structures are fabricated and utilized in [6–8]. Son et al. [9], also employed V-notched hydrogel sheets to construct a macro-scale 3D cell culture system. As another example, Cheng et al. [10] synthesized notched light driven gel valves that can control the flow rate via out of plane notch deformations. On the other hand, due to their large solvent content, gels are brittle materials [11]. Therefore, these soft materials are vulnerable to stress concentrators as the likely places of fracture initiation. Consequently, a throughout understanding of the gel fracture is highly important. To this end, a deep knowledge of the stress and solvent concentration fields around the concentrator is crucial.

The singular stress and solvent concentration fields in cracked gels have been the subject of many recent research works. Hui et al. [12], for instance, studied the asymptotic time-dependent stress and deformation fields around the tip of a mode I plane stress crack in a hydrogel. These researchers showed that the stress component normal to the crack line have a $1/r$ singularity (see Fig. 1) and the crack profile becomes a

* Corresponding authors.
E-mail addresses: yunlong@buaa.edu.cn (Y. Li), chenxianjia@lnm.imech.ac.cn (X. Chen).

https://doi.org/10.1016/j.tafmec.2021.103122
Received 7 April 2021; Received in revised form 3 September 2021; Accepted 7 October 2021
Available online 11 October 2021

Nomenclature

a	Notch depth
A_n	$(n = 1,2,..)$Mode I coefficients of the notch tip asymptotic fields
B_n	$(n = 1,2,..)$Mode II coefficients of the notch tip asymptotic fields
c	Number of solvent molecules per unit gel volume
c_0	Initial solvent concentration
$f_n(\theta)$	Unknown function ofθ
G	Shear modulus
K_V^I	Mode I notch stress intensity factor
K_V^{II}	Mode II notch stress intensity factor
k_B	Boltzmann constant
M	Number of terms considered in the truncated series of the asymptotic solutions
N	Number of polymer chains per unit reference volume
r,θ	Polar coordinate components
T	Absolute temperature
u_1, u_2	Far field applied small displacements
V	Deformed gel volume
W	Specimen width
x, y	Cartesian coordinate components
β_n^I, β_n^{II}	nth mode I and mode II eigenvalues
γ	Notch opening angle
ε_{ij}	Strain Fields
ε_{kk}	Volumetric part of the strain fields
λ_0	Initial swelling ratio
μ_0	Solvent chemical potential
ν	Poisson's ratio
ρ	Parameter related to the notch angle
σ_{rr}, $\sigma_{\theta\theta}$,$\sigma_{r\theta}$	Notch tip stresses in polar coordinate
$\varnothing$	Airy stress function
χ	Flory–Huggins interaction parameter
Ω	Volume of one solvent molecule

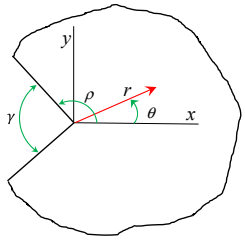

Fig. 1. Schematic representation of a sharp V-notch with the associated polar coordinates.

parabolic upon deformation. The same researchers in a similar work [13] studied asymptotic stress fields around a mode III or anti-plane shear crack in a double network hydrogel. They found that for the special case of Gaussian polymer chains (i.e. with neo-Hookean strain energy), the asymptotic stress fields show a square-root singularity (i.e $\sigma \propto r^{-0.5}$). In another work, Bouklas et al. [14] explored the transient asymptotic mode I stress fields in a cracked plane strain gel and showed that the stress singularity depends on the solvent diffusion. According to these authors, in the early stages, stress singularity is strong ($\sigma \propto r^{-1}$) and then becomes weaker ($\sigma \propto r^{-0.5}$) due to solvent diffusion around the crack. Solvent diffusion, is, indeed, an important factor in crack propagation in gels which leads to interesting phenomena like poroelastic toughening and delayed fracture [15–17]. Apart from these large deformation studies, for the sake of both numerical and theoretical convenience, linear poroelasticity has also been frequently utilized by researchers to examine the asymptotic fields around cracked gels which are reviewed next.

Hui and his co-workers [18] studied the short time transient stress fields around a plane strain stationary crack under opening deformation mode when a sudden load is applied to a poroelastic solid. In these conditions, stress relaxations due to solvent flow are confined to a small region near the crack tip as the fluid molecules far from the tip do not have enough time to flow. This situation leads to a square-root singularity for the near crack tip stresses [18]. Similar results were obtained for near crack tip fields in a poroviscoelastic plane strain solid using finite element method by Yang and Lin [19]. Furthermore, Yu et al. [20] using linear poroelasticity theory presented an asymptotic analysis for a steady state growing mode I plane strain crack in a polymer gel. These researchers concluded that the near crack tip stress singularity is the same as that in the linear elastic crack tip solution (i.e. square-root singularity). Moreover, Yu et al. [21] employed linear poroelasticity theory to explore the transient asymptotic fields around a stationary mode I plane strain crack. They showed that the stress and solvent concentration fields possess the same order of singularity while the solvent chemical potential is not singular at the crack tip. It should be noted that all the aforementioned works studied plane strain cracks while, experimentally, thin sheet samples are used to study gel fracture and thus plane stress conditions prevail. Pure shear test is, as an example, close to plane stress conditions. Consequently, Yu et al. [16], in another work, studied the subtle differences between plane strain and plane stress conditions employing linear poroelasticity theory. It was shown that the plane stress solvent concentration field depends on both in-plane normal strains and the chemical potential.

The literature review shows that the available works are limited to cracked gels which are special cases of sharp corners. The only exception, is our recent work [22] in which we have studied asymptotic fields around stationary sharp V-notches with different opening angles employing linear poroelasticity theory. In this work, we have shown that near notch tip stress fields possess the same singularity as their corresponding linear elasticity solution. All of these researches, however, are restricted to pure mode I or mode III loading conditions and, to the best of our knowledge, there is no work available focusing on mixed mode fracture of gels. To fill this gap, the present work is devoted to theoretical and numerical study of the equilibrium near notch tip stress and concentration fields under in-plane mixed mode loadings. To this end, in the next section, we will obtain the near notch tip asymptotic stress and solvent concentration fields by solving equilibrium equations utilizing the Airy stress approach. Section 3, on the other hand, is devoted to finite element investigation of the asymptotic solution to verify its applicability and accuracy. Section 4, finally, summarizes the main findings of the present study.

2. Linear poroelastic analysis of a stationary notch

Consider a freely swollen gel in the initial state which is completely immersed in a solvent. If λ_0 denotes the swelling ratio of the gel relative to its dry state, and in addition, μ_0 represents the chemical potential of the solvent, the following equation states the relation of these two parameters with the gel material parameters [23]:

$$\frac{\mu_0}{k_B T} = \ln\left(\frac{\lambda_0^3 - 1}{\lambda_0^3}\right) + \frac{1}{\lambda_0^3} + \frac{\chi}{\lambda_0^6} + N\Omega\left(\frac{1}{\lambda_0} - \frac{1}{\lambda_0^3}\right) \tag{1}$$

where k_B, χ and T show the Boltzmann constant, the Flory–Huggins

interaction parameter and absolute temperature, respectively. Moreover, N and Ω denote the number of polymer chains per unit reference volume and the volume of one solvent molecule, respectively. It can be proven that under small deformation conditions, the following relation is established between the Cauchy stress and the strain fields [24]:

$$\sigma_{ij} = 2G\left(\varepsilon_{ij} + \frac{\nu}{1-2\nu}\varepsilon_{kk}\delta_{ij}\right) \tag{2}$$

where ν and G denote the Poisson's ratio and shear modulus of the gel which can be obtained from the following equations:

$$G = \frac{Nk_BT}{\lambda_0} \tag{3a}$$

$$\nu = \frac{1}{2} - \frac{N\Omega}{2}\left[\frac{1}{\lambda_0^2(\lambda_0^3-1)} + \frac{N\Omega}{\lambda_0^2} - \frac{2\chi}{\lambda_0^5}\right]^{-1} \tag{3b}$$

In addition, the volumetric part of the strain fields (ε_{kk}), which appears in Eq. (2), is related to the solvent concentration changes as follows:

$$\varepsilon_{kk} = \Omega(c - c_0) \tag{4}$$

where c and c_0 represent the number of solvent molecules per unit gel volume (i.e. solvent concentration) in the deformed and initial states of the gel, respectively. Furthermore, the initial solvent concentration is related to the initial swelling ratio as $\Omega c_0 = 1 - \lambda_0^{-3}$.

On the other hand, in the absence of body and inertial forces, the given stress fields σ_{ij} in Eq. (2) should satisfy the following mechanical equilibrium equation:

$$\frac{\partial \sigma_{ij}}{\partial x_j} = 0 \tag{5}$$

In addition to Eq. (5), the solvent concentration field should also satisfy the following equation to guarantee the chemical equilibrium of the gel [24]:

$$\nabla^2 c = 0 \tag{6}$$

For small deformations, Eqs. (5) and (6) are the main governing equations of the gel thermodynamic equilibrium based on the linear poroelasticity theory. More details about the derivation of these equations from the original Biot's poroelasticity theory can be found in [24]. These equations, therefore, should be solved employing proper boundary conditions to extract the equilibrium stress and solvent concentration fields around sharp V-notches. It can be observed that these equations are decoupled and thus can be solved independently. Furthermore, one may note that if the stress fields have been calculated, employing Eqs. (2) and (4), the solvent concentration field can also be determined accordingly. This concentration field should also certainly satisfy the chemical equilibrium equation (i.e. Eq. (6)). Therefore, first, we solve the mechanical equilibrium equations.

To solve the mechanical equilibrium equations, similar to two-dimensional linear elasticity problems, we employ the Airy stress function $\varnothing(r,\theta)$ which is related to different stress components in polar coordinates as follows:

$$\sigma_\theta = \frac{\partial^2 \varnothing}{\partial r^2}, \sigma_{r\theta} = -\frac{\partial}{\partial r}\left(\frac{1}{r}\frac{\partial \varnothing}{\partial \theta}\right), \sigma_r = \frac{1}{r}\frac{\partial \varnothing}{\partial r} + \frac{1}{r^2}\frac{\partial^2 \varnothing}{\partial \theta^2} \tag{7}$$

It can be checked that by the above definition, mechanical equilibrium equations are satisfied automatically and we should only find the proper form of the Airy stress function. To this end, we note that the stress function should be a biharmonic one to guarantee the solution compatibility which means that we should solve:

$$\nabla^4 \varnothing = 0 \tag{8}$$

instead of the original mechanical equilibrium equations. After finding the stress function, we can utilize Eqs. (2) and (4) in order to determine the concentration field. Doing so, the following relation is obtained between the concentration field and the stress function:

$$\begin{cases} (c - c_0) = \dfrac{0.5-\nu}{(1+\nu)G\Omega}\nabla^2 \varnothing planestress \\ (c - c_0) = \dfrac{0.5-\nu}{G\Omega}\nabla^2 \varnothing planestrain \end{cases} \tag{9}$$

From this equation, it is clear that since the stress function is a biharmonic one, the chemical equilibrium equation would also be automatically satisfied using the Airy stress function approach. In the next subsection, we will employ this approach to study equilibrium asymptotic stress and concentration fields around sharp V-notches under in-plane mixed mode loadings in polymer gel samples. Here it should be noted that the obtained asymptotic fields in the present study are valid when the gel body deforms close to its equilibrium states. These conditions realize when the mechanical loads are applied sufficiently slow to the gel specimens (e.g. [25,26]) to avoid dynamic effects like poroelastic toughening or viscoelastic deformations.

2.1. Asymptotic analysis

This subsection is devoted to obtaining the equilibrium stress and solvent concentration fields around a stationary sharp V-notch subjected to mixed mode (I/II) deformations. Consider a typical notched sample, as shown schematically in Fig. 1 with the polar coordinates $(r-\theta)$ attached to the notch tip, where r and θ are the radial and tangential coordinates, respectively. Based on Fig. 1, γ shows the notch opening angle which can be written in terms of ρ as $\gamma = 2\pi - 2\rho$.

Next following Williams' solution [27] for linear elastic problems, we assume the following multiplicative form for the stress function $\varnothing$:

$$\varnothing(r,\theta) = \sum_{n=1} r^{\beta_n+1} f_n(\theta) \tag{10}$$

This function should satisfy the biharmonic equation in the polar coordinates which is:

$$\nabla^4 \varnothing = \left(\frac{\partial^2}{\partial r^2} + \frac{1}{r}\frac{\partial}{\partial r} + \frac{1}{r^2}\frac{\partial^2}{\partial \theta^2}\right)\left(\frac{\partial^2 \varnothing}{\partial r^2} + \frac{1}{r}\frac{\partial \varnothing}{\partial r} + \frac{1}{r^2}\frac{\partial^2 \varnothing}{\partial \theta^2}\right) \tag{11}$$

Thus, by substituting Eq. (10) into Eq. (11) and after some simplifications, one can obtain the following fourth order differential equation for the unknown function $f_n(\theta)$:

$$f_n^{''''}(\theta) + 2\left(1+\beta_n^2\right)f_n^{''}(\theta) + \left(\beta_n^2 - 1\right)^2 f_n(\theta) = 0 \tag{12}$$

with the following solution:

$$f_n(\theta) = A_n\cos((1+\beta_n)\theta) + B_n\sin((1+\beta_n)\theta) + D_n\cos((\beta_n-1)\theta) + E_n\sin((\beta_n-1)\theta) \tag{13}$$

By substitution of this solution into Eq. (7), one can obtain the stress components around the notch tip in terms of $f_n(\theta)$ as follows:

$$\sigma_{\theta\theta} = \beta_n(\beta_n+1)r^{\beta_n-1}f_n(\theta) \tag{14a}$$

$$\sigma_{rr} = r^{\beta_n-1}\left[(\beta_n+1)f_n(\theta) + f_n^{''}(\theta)\right] \tag{14b}$$

$$\sigma_{r\theta} = -\beta_n r^{\beta_n-1} f_n^{'}(\theta) \tag{14c}$$

These stress components should satisfy the following traction free boundary conditions:

$$\begin{cases} \sigma_{\theta\theta}|_{\theta=\rho} = 0 \rightarrow f_n(\rho) = 0 \\ \sigma_{\theta\theta}|_{\theta=-\rho} = 0 \rightarrow f_n(-\rho) = 0 \\ \sigma_{r\theta}|_{\theta=\rho} = 0 \rightarrow f_n^{'}(\rho) = 0 \\ \sigma_{r\theta}|_{\theta=-\rho} = 0 \rightarrow f_n^{'}(-\rho) = 0 \end{cases} \tag{15}$$

These boundary conditions lead to a system of homogeneous equations which is essentially an eigenvalue problem with the following two

independent characteristic equations:

$$\beta_n^I sin(2\rho) + sin\left(2\rho\beta_n^I\right) = 0 \tag{16a}$$

$$\beta_n^{II} sin(2\rho) - sin\left(2\rho\beta_n^{II}\right) = 0 \tag{16b}$$

in which the superscripts of "*I*" and "*II*" are added to denote the eigenvalues related to mode I and mode II loadings, respectively. It can be checked that the first characteristic equation comes from the first two boundary conditions for the circumferential stress while the second characteristic equation is a result of the last two boundary conditions for the shear stress component $\sigma_{r\theta}$.Therefore, Eqs. (16a) and (16b) determine the eigenvalues related to the symmetric (mode I) and antisymmetric (mode II) modes of deformation, respectively.

Fig. 2a and 2b show the variations of the first three eigenvalues of mode I and mode II against the notch opening angle, respectively. Based on this figure, while the first eigenvalues for both modes of deformation are real numbers, the higher order ones can be complex numbers depending on the notch opening angle. Furthermore, it is clear that the first mode I eigenvalue is always less than one and hence, based on Eq. (14), the corresponding stress components are singular accordingly. For mode II deformations, however, the first eigenvalue is larger than one for opening angles greater than about 102° and hence the associated stress fields would not be singular. Here, it should be mentioned that the characteristic equation for mode II deformations (i.e. Eq. (16b)) also admits $\beta_n^{II} = 1$ as a solution for all notch angles. However, the associated term to this eigenvalue shows rigid body rotations of the notch around its tip and thus does not contribute to the notch tip stress and strain fields. Therefore, we have not plotted this eigenvalue in Fig. 2b. More details about this rigid body rotation and plots similar to Fig. 2 can be found in [28,29]. Finally, note that in Fig. 2 and throughout the paper the notations Re(■) and Im(■) denote the real and imaginary parts of (■), respectively.

After some simplifications, it can be shown that the stress function ∅ can be obtained as follows:

$$\varnothing(r,\theta) = r^{\beta_n^I+1}A_n\left[\cos\left(\left(\beta_n^I-1\right)\theta\right) - \frac{\beta_n^I\cos(2\alpha)+\cos(2\beta_n^I\alpha)}{\left(\beta_n^I+1\right)}\cos\left(\left(\beta_n^I+1\right)\theta\right)\right] + r^{\beta_n^{II}+1}B_n\left[\sin\left(\left(\beta_n^{II}-1\right)\theta\right) + \frac{\cos\left(2\beta_n^{II}\alpha\right)-\beta_n^{II}\cos(2\alpha)}{\left(\beta_n^{II}+1\right)}\sin\left(\left(\beta_n^{II}+1\right)\theta\right)\right] \tag{17}$$

and thus the stress fields near the notch tip loaded in mixed mode (I/II) conditions, considering Eq. (7), can be achieved as follows:

$$\begin{Bmatrix}\sigma_{rr}\\ \sigma_{\theta\theta}\\ \sigma_{r\theta}\end{Bmatrix} = \sum_{n=1} Re\left(\frac{\beta_n^I A_n}{r^{1-\beta_n^I}}\begin{Bmatrix}(3-\beta_n^I)\cos\left(\left(\beta_n^I-1\right)\theta\right)+\left(\cos\left(2\beta_n^I\rho\right)+\beta_n^I\cos(2\rho)\right)\cos\left(\left(\beta_n^I+1\right)\theta\right)\\ \left(\beta_n^I+1\right)\cos\left(\left(\beta_n^I-1\right)\theta\right)-\left(\cos\left(2\beta_n^I\rho\right)+\beta_n^I\cos(2\rho)\right)\cos\left(\left(\beta_n^I+1\right)\theta\right)\\ \left(\beta_n^I-1\right)\sin\left(\left(\beta_n^I-1\right)\theta\right)-\left(\cos\left(2\beta_n^I\rho\right)+\beta_n^I\cos(2\rho)\right)\sin\left(\left(\beta_n^I+1\right)\theta\right)\end{Bmatrix}\right)$$
$$-\sum_{n=1} Re\left(\frac{\beta_n^{II} B_n}{r^{1-\beta_n^{II}}}\begin{Bmatrix}(3-\beta_n^{II})\sin\left(\left(\beta_n^{II}-1\right)\theta\right)-\left(\cos\left(2\beta_n^{II}\rho\right)-\beta_n^{II}\cos(2\rho)\right)\sin\left(\left(\beta_n^{II}+1\right)\theta\right)\\ \left(\beta_n^{II}+1\right)\sin\left(\left(\beta_n^{II}-1\right)\theta\right)+\left(\cos\left(2\beta_n^{II}\rho\right)-\beta_n^{II}\cos(2\rho)\right)\sin\left(\left(\beta_n^{II}+1\right)\theta\right)\\ \left(1-\beta_n^{II}\right)\cos\left(\left(\beta_n^{II}-1\right)\theta\right)-\left(\cos\left(2\beta_n^{II}\rho\right)-\beta_n^{II}\cos(2\rho)\right)\cos\left(\left(\beta_n^{II}+1\right)\theta\right)\end{Bmatrix}\right) \tag{18}$$

which is similar to the linear elastic solution for sharp V-notches where the first summation is for mode I while the second summation calculates the mode II contributions to the stress fields. For complete determination of the stress fields in the proximity of the notch tip, the unknown coefficients A_n and B_n should be obtained from the loading and geometry conditions. Similar to linear elastic fracture mechanics (LEFM), we relate the singular terms A_1 and B_1 with the mode I and mode II notch stress intensity factors (i.e., K_V^I and K_V^{II}) as follows:

$$\begin{cases} K_V^I = \lim_{r\to 0}\left(\sqrt{2\pi}\, r^{1-\beta_1^I}\times\sigma_{\theta\theta}(\theta=0)\right) = \sqrt{2\pi}\,\beta_1^I\left(1+\beta_1^I-\beta_1^I\cos(2\rho)-\cos(2\rho\beta_n^I)\right)A_1 \\ K_V^{II} = \lim_{r\to 0}\left(\sqrt{2\pi}\, r^{1-\beta_1^{II}}\times\sigma_{r\theta}(\theta=0)\right) = \sqrt{2\pi}\,\beta_1^{II}\left(\beta_1^{II}-1-\beta_1^{II}\cos(2\rho)+\cos(2\rho\beta_1^{II})\right)B_1 \end{cases} \tag{19}$$

On the other hand, by substitution of Eq. (17) into Eq. (9), the following relation will be obtained for the solvent concentration field:

$$(c-c_0)=\begin{cases}\sum_{n=1} Re\left(\frac{2(1-2\nu)}{(1+\nu)G\Omega}\left(\frac{\beta_n^I A_n}{r^{1-\beta_n^I}}\cos\left((\beta_n^I-1)\theta\right)-\frac{\beta_n^{II}B_n}{r^{1-\beta_n^{II}}}\sin\left((\beta_n^{II}-1)\theta\right)\right)\right) planestress\\ \sum_{n=1} Re\left(\frac{2(1-2\nu)}{G\Omega}\left(\frac{\beta_n^I A_n}{r^{1-\beta_n^I}}\cos\left((\beta_n^I-1)\theta\right)-\frac{\beta_n^{II}B_n}{r^{1-\beta_n^{II}}}\sin\left((\beta_n^{II}-1)\theta\right)\right)\right) planestrain\end{cases} \tag{20}$$

which shows that mode I and mode II deformations exhibit cosine and sine variations with respect to the angular coordinates, respectively.

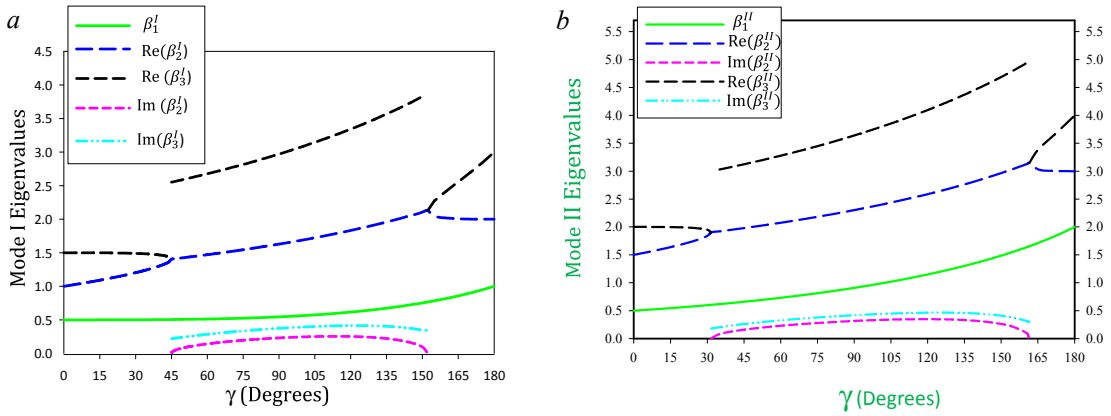

Fig. 2. The first three eigenvalues of *a*) mode I and *b*) mode II against the notch opening angle.

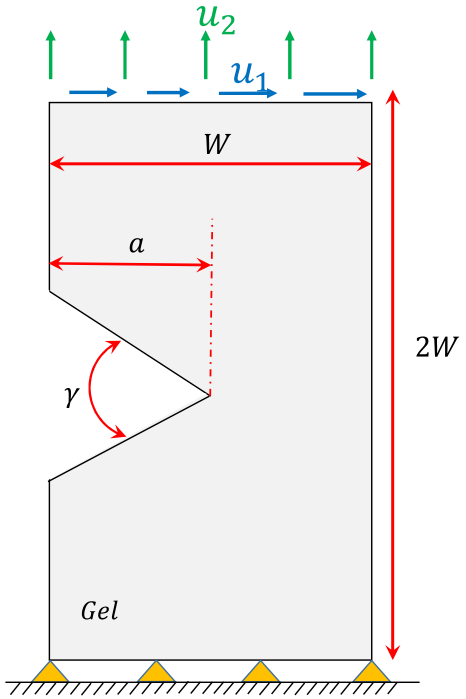

Fig. 3. Schematic representation of the single edge notch sample, loaded in the shear-tension (i.e., mixed-mode I/II) loading condition.

This means that adding shear deformations to the near notch tip region will break the symmetry of the solvent distribution around the notch tip with respect to the notch bisector line. It is here worth mentioning that the near notch tip solvent concentration field can be obtained through any of Eqs. (20), (9) or (4) which are theoretically equivalent. Applicability of these equations, however, depends on the available information from the field. For example, if we have already calculated the coefficients A_n and B_n, it is easier to employ Eq. (20) while Eq. (4) would be more convenient if we have the notch deformation fields as in finite element simulations. Summarily, Eqs. (18) and (20) are the asymptotic stress and solvent concentration fields around the notch tip with the specified boundary conditions in Eq. (15). In the next section, we will

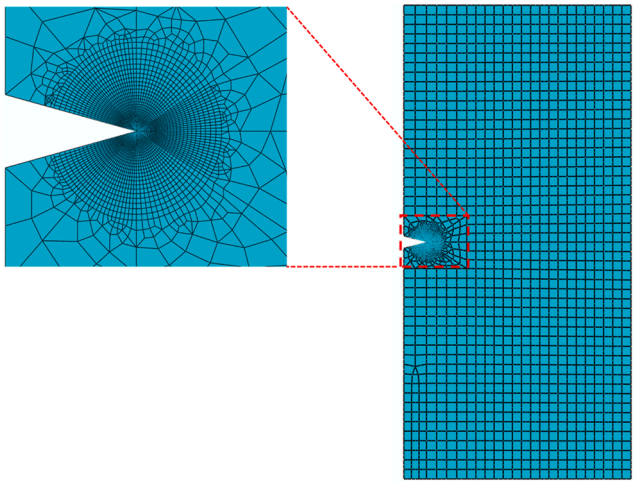

Fig. 4. A typical mesh pattern utilized in the finite element analyses of sharp V-notches with $\gamma = 30^o$and $a/W = 0.1$.

Table 1
Geometry and material properties of the SEN samples.

Parameter	Value
a/W	0.1
γ	30°, 60°
$G\Omega/k_BT$	3×10^{-4}
ν	0.24

explore the accuracy of these analytical fields with their corresponding numerical results obtained from the finite element method for different notch angles under mixed mode I/II loadings.

Finally, it should be mentioned that although the obtained stress field equations are similar to their corresponding results of linear elasticity theory [30–34], there is an essential difference between the two solutions. Linear elastic solutions are valid for single phase materials while the present solution is applicable to polymeric gels which have two phases, namely polymeric network and the diffusing solvent molecules. In fact, in gels, solvent diffusion is coupled to the network deformation and hence can affect the fracture behavior of the network as well. This fact will be discussed in more details later. Therefore, the results of Eq. (20) which are irrelevant for linear elastic materials is an important difference between linear elasticity and poroelasticity theories. The solutions of the linear elasticity and poroelasticity theories become the same if we can ignore the effects of the solvent phase. This condition realizes, for example, if the loading rate is so much fast that the solvent molecules do not have enough time to diffuse and redistribute inside the gel. In these conditions, the gel will behave as an incompressible elastic material with $c = c_0$ everywhere and thus our equilibrium solution does not apply.

3. Numerical results and discussion

In this section, the near notch tip stress and solvent concentration fields are calculated using finite element method and the obtained results are compared with the predictions of the present asymptotic solution to verify its accuracy. To this end, SEN samples made from polymer gels subjected to mixed mode deformations are modeled in ABAQUS finite element code for both plane stress and plane strain conditions. Fig. 3 shows a schematic representation of this specimen.

Based on this figure, parameters W, a and γ denote the sample width,

Table 2
The first three mode I and II eigenvalues and their corresponding asymptotic coefficients of the 30° SEN specimen under plane stress conditions with $u_1/a = 0.018$ and $u_2/a = 0.002$.

Parameter	Value
β_1^I	0.5015
$A_1 a^{\beta_1^I - 1}\Omega/k_BT$	6.0336×10^{-8}
β_2^I	1.2030
$A_2 a^{\beta_2^I - 1}\Omega/k_BT$	-1.3687×10^{-8}
β_3^I	1.4904
$A_3 a^{\beta_3^I - 1}\Omega/k_BT$	1.1063×10^{-8}
β_1^{II}	0.5982
$B_1 a^{\beta_1^{II} - 1}\Omega/k_BT$	-3.4422×10^{-8}
β_2^{II}	1.8389
$B_2 a^{\beta_2^{II} - 1}\Omega/k_BT$	-5.9680×10^{-8}
β_3^{II}	1.9486
$B_3 a^{\beta_3^{II} - 1}\Omega/k_BT$	5.7750×10^{-8}

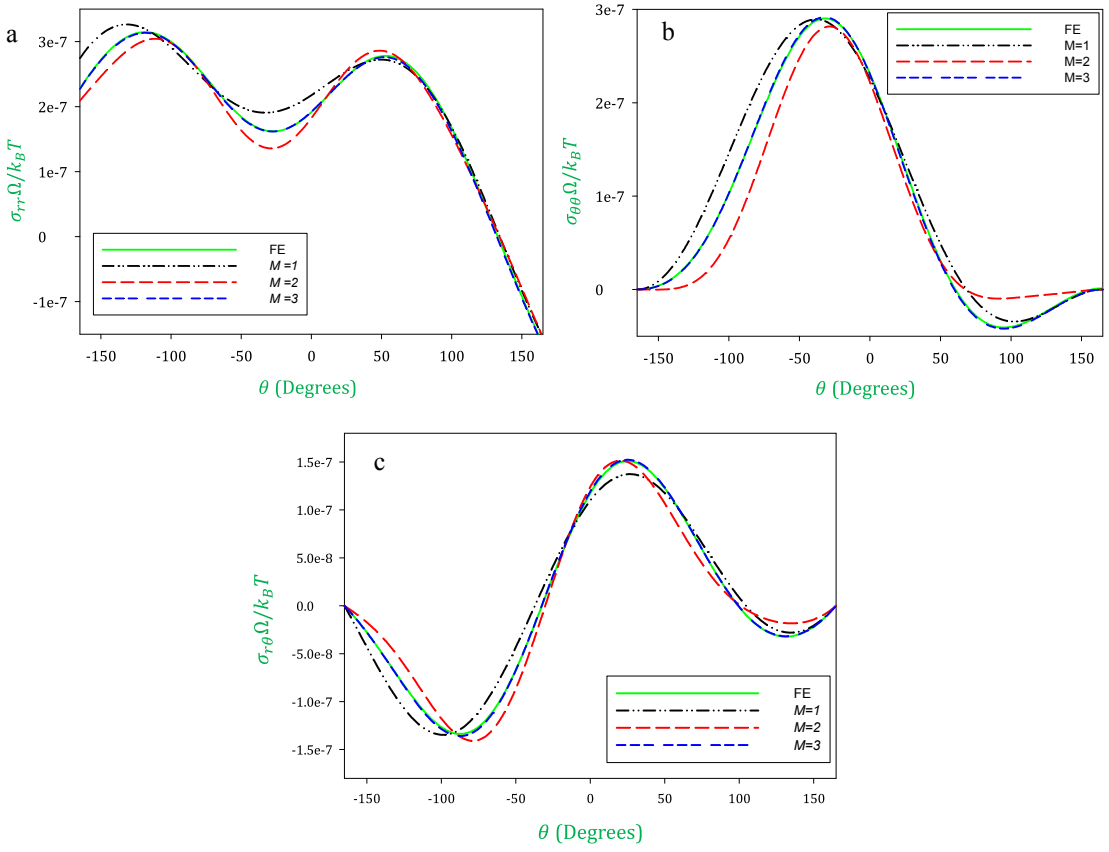

Fig. 5. Comparison between the FE solution and the presented asymptotic solutions for a 30° plane stress notch with $M = 1,2$ and 3 : a) radial b) tangential and c) shear stress components versus θ on a ring around the notch tip with $r/a = 0.08$. The applied boundary displacements are $u_1/a = 0.018$ and $u_2/a = 0.002$.

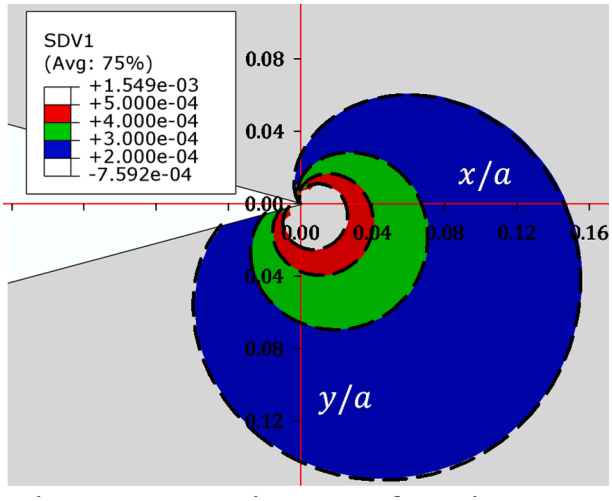

Fig. 6. Comparison between the reconstructed contours from the asymptotic solution with $M = 3$ and the finite element results for the dimensionless solvent concentrations of $c\Omega = 2 \times 10^{-4}$, 3×10^{-4}, 4×10^{-4} and 5×10^{-4} in a 30° notched gel for the applied boundary displacements of $u_1/a = 0.018 \text{and} u_2/a = 0.002$.

notch depth and the notch opening angle, respectively while u_1 and u_2 show the far field applied small displacements to the specimen to induce mixed mode conditions around the notch tip. To be more precise, the mode mixity of the notch tip deformations can be controlled by changing the ratio of u_1/u_2. Indeed, by increasing this ratio from zero to big numbers, the near notch tip deformations change from pure mode I to mixed mode conditions. Furthermore, to model the gel equilibrium behavior under small strains, the UHYPER subroutine presented by [35] is employed in our study. This subroutine provides the gel strain energy density and its derivatives to ABAQUS which in effect, for small strains, results in the material behavior given in Eqs. (2) to (4).

Furthermore, Fig. 4 shows a typical mesh pattern used for the finite element analyses. As it can be seen, due to the high stress/solvent concentration gradients close to the notch tip, a very fine mesh is employed in this region. In fact, six-node quadratic triangular elements with reduced integration (CPS6R or CPE6R) are utilized for the first row of elements around the notch apex while for the rest of the near notch tip region (i.e. inside the circle) eight-node quadratic quadrilateral elements with reduced integration (CPS8R or CPE8R) are used. Furthermore, as schematically shown in Fig. 3, the far field small displacements are applied to the upper horizontal edge of the specimen while the lower horizontal edge is fixed to eliminate possible rigid body motions.

Table 1 gives the geometry and material parameters considered in the finite element analyses. Based on this table, two notch opening angles, namely 30° and 60° are considered for the analyses. Here, it should be noted that the UHYPER subroutine needs $N\Omega$ and χ as the input parameters which are related to the gel material properties (given in Table 1) according to Eqs. (3a) and (3b). It can be checked that these values are 0.001 and 0.2, respectively which leads to $\lambda_0 = 3.215$ for $\mu_0 = 0$.

Table 3
The first two mixed mode eigenvalues and the corresponding asymptotic coefficients of the 60° SEN specimen under plane strain conditions with $u_1/a = 0.018 \text{and} u2/a = 0.002$.

Parameter	Real Part	Imaginary Part
β_1^I	0.5122	0
$A_1 a^{\beta_1^I - 1}\Omega/k_B T$	6.1802×10^{-8}	0
β_2^I	1.4710	0.1419
$A_2 a^{\beta_2^I - 1}\Omega/k_B T$	-1.6818×10^{-9}	-2.2071×10^{-8}
β_1^{II}	0.7309	0
$B_1 a^{\beta_1^{II} - 1}\Omega/k_B T$	-5.4755×10^{-8}	0
β_2^{II}	2.0748	0.2294
$B_2 a^{\beta_2^{II} - 1}\Omega/k_B T$	-2.5144×10^{-9}	1.7536×10^{-8}

After explaining the finite element model details, we focus on the present asymptotic solution. This solution has a series form with infinite terms and hence it is needed to utilize a truncated form of this solution with M terms. Clearly, for a specified radial distance from the notch tip, by increasing M, the solution accuracy should also increase. Therefore, there is a true need for a reliable and applicable algorithm to calculate any desired number of coefficients A_n andB_n. Among available algorithms, the finite element over deterministic (FEOD) method proposed by [29] which has been widely applied in previous studies (e.g. [22,36–38]), is utilized in the current research due to its proven simplicity and accuracy. In this method, first, the notched sample should be modeled in a finite element code. Then, the nodal coordinates and displacements are extracted from the nodes closed to the notch tip. Next, these nodal values should be substituted into the series solution of the displacement fields and as a result an over-determined set of linear equations is achieved. Employing the least-squares method, finally, the nodal displacements reduce to a small set of unknown coefficients (i.e., A_n and B_n) which can be calculated accordingly. For more details about this approach, one can refer to [29].

Fig. 5a to 5c illustrate variations of different stress components near the notch tip for the 30° SEN specimen with the angular coordinate θ obtained from the asymptotic solution (i.e. Eq. (18)) with one, two and three terms in comparison with the finite element results. The corresponding first three eigenvalues of mode I and mode II and their associated coefficients A_n and B_n obtained from the FEOD method are also given in Table. 2. The stress components are calculated at the radial distance of $r/a = 0.08$ and under plane stress conditions. The applied boundary displacements are, furthermore, $u_1/a = 0.018$ and $u_2/a = 0.002$. According to Fig. 5, the asymptotic solution can accurately capture variations of all the stress components at the radial distance of $r/a = 0.08$ by considering only the first three terms of the truncated mode I and mode II solutions. Here it should be noted that none of the stress components are symmetric with respect to the notch bisector line (i.e. $\theta = 0$) which implies that mode II deformations have a considerable contribution to the near notch tip stresses. This fact can also be observed from the magnitudes of mode II coefficients B_1 to B_3 in Table. 2 which are in the same order of their corresponding values for mode I coefficients A_1 to A_3, respectively.

Now and after validation of the stress fields, it is of interest to compare the predictions of the asymptotic solution for the solvent concentration field (i.e. Eq. (20)) in the proximity of notch tip with its corresponding finite element data. To do so, we consider again the plane stress 30° SEN gel sample with the previous applied boundary displacements (i.e., $u_1/a = 0.018 \text{and} u_2/a = 0.002$). For this specimen, considering the first three terms of the mixed mode asymptotic solution (i.e. Eq. (20) with $M = 3$) with the given coefficients in Table. 2, one may reconstruct contours of the dimensionless solvent concentration (i.e. $c\Omega$) close to the notch apex. These contours are illustrated in Fig. 6 in dashed black lines for the typical values of $c\Omega = 2 \times 10^{-4}$, 3×10^{-4}, 4×10^{-4} and 5×10^{-4} in comparison with their corresponding finite element results. In this figure, SDV1 is a state variable which is defined and calculated in the subroutine UHYPER. To be more precise, based on Eq. (4), solvent concentration is related to the gel volume change (i.e. ε_{kk}). On the other hand, this volume change can be calculated using variable "AJ" which is passed in by ABAQUS in UHYPER subroutines [39]. This variable, at any material point, based on the formulation given in [35], shows the ratio of deformed gel volume V to its initial value λ_0^3 (i.e. $AJ = V/\lambda_0^3$). Therefore, by defining SDV1=$AJ - 1 = \varepsilon_{kk}$, we can simply calculate the solvent concentration. According to Fig. 6, it is clear that the present asymptotic solution with three terms can accurately predict the solvent

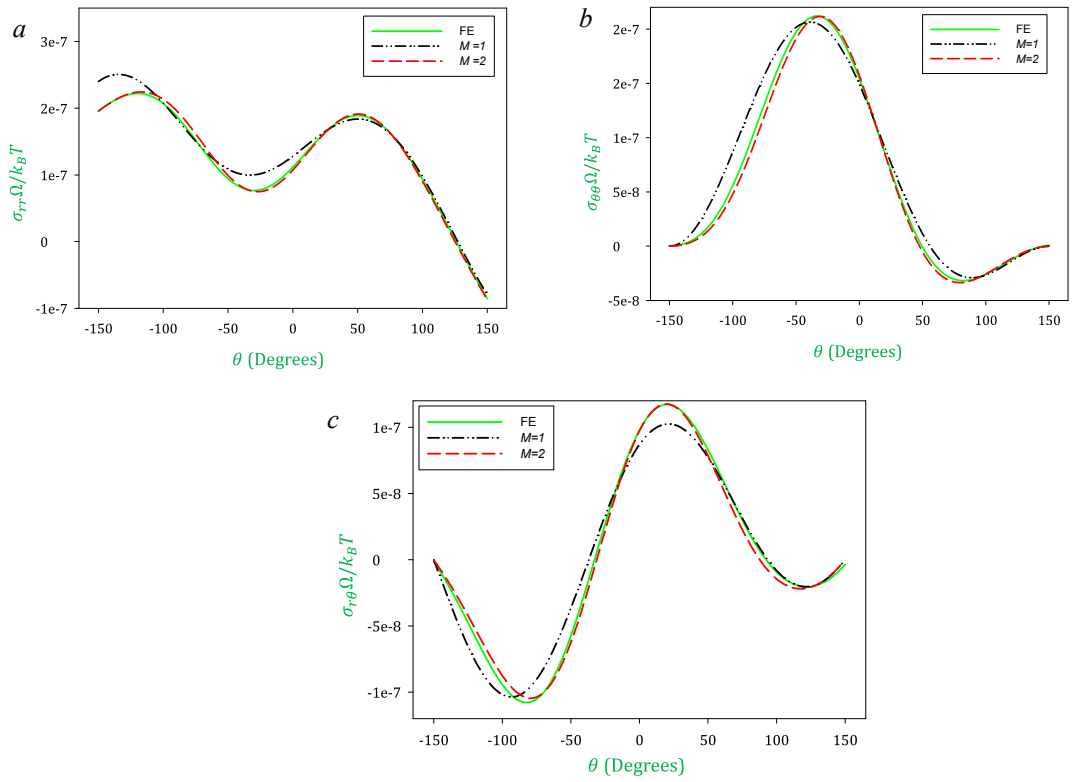

Fig. 7. Comparison between the FE results and the present asymptotic solutions for a 60° plane strain notch with $M = 1, 2$: a) radial b) tangential and c) shear stress components versus θ on a ring around the notch tip with $r/a = 0.2$. The applied boundary displacements are $u_1/a = 0.018 \text{and} u_2/a = 0.002$.

Table 4
The first two mode I asymptotic coefficients of the 60° SEN specimen under plane strain conditions with $u_1/a = 0 \text{and} u2/a = 0.002$.

Parameter	Real Part	Imaginary Part
$\boldsymbol{A_1 a^{\beta_1^I - 1} \Omega / k_B T}$	5.6874×10^{-8}	0
$\boldsymbol{A_2 a^{\beta_2^I - 1} \Omega / k_B T}$	-6.0301×10^{-9}	-2.1518×10^{-8}

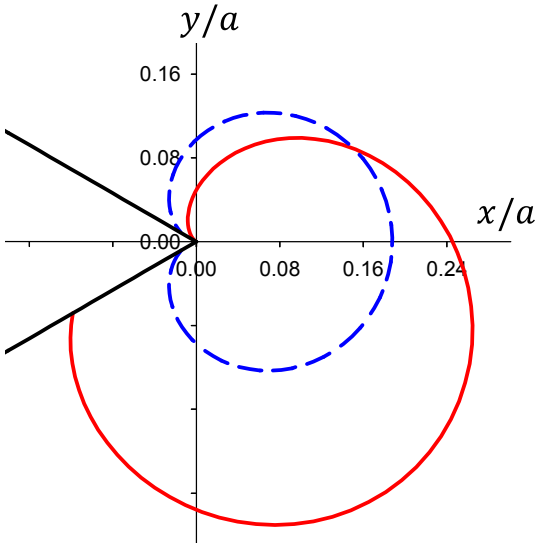

Fig. 8. Comparison between the reconstructed contours of the solvent concentration around the plane strain notch tip of the 60° SEN specimen under pure mode I (dashed line) and mixed mode (full line) loading conditions. The contours are plotted for the typical value of $c\Omega = 2 \times 10^{-4}$.

concentration field around the notch tip up to radial distances of about $r/a = 0.16$. Furthermore, from Fig. 6, it can be observed that the pore pressure field around the notch tip is not symmetric with respect to the notch bisector line and is, in fact, rotated due to anti-symmetric (mode II) deformations.

For the sake of more verification, we next consider a 60° SEN sample made of the polymer gel with the material and geometry parameters given in Table. 1 and under plane strain conditions. For this sample, employing the FEOD method, the first two mixed mode eigenvalues and their corresponding coefficients are calculated and reported in Table. 3. Utilizing these coefficients and the asymptotic solution given in Eq. (18) with $M = 2$, one may calculate the in-plane stress components, namely $\sigma_{rr}, \sigma_{\theta\theta}$ and $\sigma_{r\theta}$ as a function of polar coordinates r and θ. Fig. 7 depicts the angular variations of these stress components at a radial distance of $r/a = 0.2$ obtained from both the asymptotic solution with $M = 2$ and the finite element simulations with boundary displacements of $u_1/a = 0.018 \text{and} u_2/a = 0.002$.

According to Fig. 7, considering only the singular terms of the asymptotic solution (i.e. $M = 1$) cannot accurately capture the stress fields variations around the notch tip at the specified radial distance. Adding the first non-singular term, however, will remove the discrepancy between the finite element results and the asymptotic solution and make the predictions accurate. This result also confirms the accuracy and the applicability of the present solution for the equilibrium asymptotic fields around stationary sharp V-notches made of polymer gels under mixed mode loadings.

Let us finally explore the effects of mode mixity on the solvent concertation field around the notch tip of the 60° SEN specimen. To this end, we have repeated the finite element simulation for the applied boundary displacements of $u_1/a = 0 \text{and} u_2/a = 0.002$ which induce pure mode I loading conditions around the notch tip. Table. 4 gives the first two corresponding coefficients obtained by the FEOD method. Using these coefficients and the information provided in Table. 3 accompanied with Eq. (20), we may reconstruct contours of the solvent concentration

field for the typical value of $c\Omega = 2 \times 10^{-4}$ for both pure mode I and mixed mode loading conditions (i.e. $u_1/a = 0.018 \text{and} u_2/a = 0.002$). Fig. 8 illustrates these reconstructed contours together.

According to Fig. 8, by increasing the loading mode mixity (i.e. the ratio of u_1/u_2), the solvent concentration contour will expand and rotate around the notch tip and lose its symmetry with respect to the notch bisector line. In fact, by increasing u_1, the normal stress components (i.e. $\sigma_{rr} \text{and} \sigma_{\theta\theta}$) will increase and decrease for negative and positive values of θ, respectively. This fact can be observed from the sine terms of Eq. (18) and the coefficients given in Tables. 3. These changes in the stress components will affect the pore pressure field around the notch tip which in effect alter the solvent concentration distribution. To be more precise, upon increasing u_1, the near notch tip material points below and above the notch bisector line will be expanded and squeezed, respectively. Consequently, higher suctions will appear in the lower material points which leads to absorbing more solvent molecules to these points. This unequal distribution of solvent molecules with respect to the notch bisector line, will certainly affect the propensity of near notch tip material points to crack propagation. Indeed, more swollen points are more vulnerable to brittle fracture as they have lower number of stretched polymer chains per volume and thus needs less energy to be ruptured [40]. Clearly, a more detailed study is needed to investigate this phenomenon which would be an interesting extension of the present work.

4. Conclusion

The present work was devoted to extracting equilibrium stress and solvent concentration fields around stationary sharp V-notches made from polymer gels under mixed mode in-plane loadings utilizing linear poroelasticity theory. To this end, first, the mechanical equilibrium equations were solved employing the Airy stress function and then the near notch tip stress components were obtained accordingly. The stress fields have series forms and are similar to their corresponding linear elastic solution. Next, considering the incompressibility of the gel constituents (reflected in Eq. (4)), the solvent concentration field was obtained based on the already obtained stress components for both plane stress (thin specimens) and plane strain (thick specimens) conditions. It is found that mode I and mode II deformations have cosine and sine contributions to the solvent concentration field with respect to the angular coordinates. This means that by adding mode II deformations to the near notch tip region, the symmetry of the solvent distribution will break with respect to the notch bisector line and the solvent molecules will be pumped from one side of the bisector line to the opposite side. After that and to verify the accuracy of the obtained asymptotic fields, finite element simulations were performed on a SEN specimen with opening angles of 30° and 60° to calculate the fields numerically. The numerical results were finally compared with their corresponding asymptotic fields employing the FEOD method for mixed mode loadings. The comparison study shows that the present asymptotic solution can accurately capture the finite element results up to radial distances of $r/a = 0.2$with only two or three terms.

The main novelties of the present work can be summarized as follows: 1) For the first time, the mixed mode in-plane equilibrium stress and solvent concentration fields around sharp V-notched polymer gels were obtained theoretically. 2) These theoretical results showed that the solvent concentration and stress fields possess the same degrees of singularity around the notch tip. 3) Explicit relations were provided for calculating solvent concentration fields. These calculations can be directly done through the displacement fields obtained from finite element simulations. 4) The theoretical results indicated that shear deformations due to mode II loading can alter the propensity of the gel material points to brittle fracture by tuning their solvent content. This interesting result has substantial consequences on fracture criteria developments for notched gels under mixed mode loadings.

CRediT authorship contribution statement

Yunlong Li: Supervision, Funding acquisition, Conceptualization, Methodology. **Zheng Niu:** Software, Writing – original draft. **Xianjia Chen:** Software, Visualization, Writing – review & editing.

Declaration of Competing Interest

The authors declare that they have no known competing financial interests or personal relationships that could have appeared to influence the work reported in this paper.

Acknowledgement

This work was supported by Fundamental Research Funds for Central Universities, Beijing Advanced Discipline Center for Unmanned Aircraft System, Beijing Municipal Science and Technology Commission (No. Z191100004619006), National Nature Science Foundation of the P. R. China (No.12002014, No.11872089 and No. 11772026), Defense Industrial Technology Development Program (No. JCKY2018601B001, No. JCKY2019203A003).

References

[1] L. Ionov, Hydrogel-based actuators: possibilities and limitations, Mater. Today 17 (10) (2014) 494–503.
[2] Y. Qiu, K. Park, Environment-sensitive hydrogels for drug delivery, Adv. Drug Deliv. Rev. (2001). http://www.sciencedirect.com/science/article/pii/S0169409X01002034 (accessed March 29, 2017).
[3] R.H. Liu, Q. Yu, D.J. Beebe, Fabrication and characterization of hydrogel-based microvalves, J. Microelectromechanical Syst. 11 (2002) 45–7157.
[4] J. Zhu, R.E. Marchant, Design properties of hydrogel tissue-engineering scaffolds, Expert Rev. Med. Devices 8 (5) (2011) 607–626.
[5] T.H. Lee, J.Y. Jho, Temperature-Responsive Actuators Fabricated with PVA/PNIPAAm Interpenetrating Polymer Network Bilayers, Macromol. Res. 26 (7) (2018) 659–664.
[6] K.-U. Jeong, J.-H. Jang, D.-Y. Kim, C. Nah, J.H. Lee, M.-H. Lee, H.-J. Sun, C.-L. Wang, S.Z.D. Cheng, E.L. Thomas, Three-dimensional actuators transformed from the programmed two-dimensional structures via bending, twisting and folding mechanisms, J. Mater. Chem. 21 (19) (2011) 6824, https://doi.org/10.1039/c0jm03631e.
[7] Y.u. Cheng, K. Ren, D. Yang, J. Wei, Bilayer-type fluorescence hydrogels with intelligent response serve as temperature/pH driven soft actuators, Sensors Actuators B Chem. 255 (2018) 3117–3126.
[8] C. Ma, W. Lu, X. Yang, J. He, X. Le, L. Wang, J. Zhang, M.J. Serpe, Y. Huang, T. Chen, Bioinspired anisotropic hydrogel actuators with on–off switchable and color-tunable fluorescence behaviors, Adv. Funct. Mater. 28 (2018) 1704568 %@ 1616–301X.
[9] J. Son, C.Y. Bae, J.-K. Park, Construction of modular hydrogel sheets for micropatterned macro-scaled 3D cellular architecture, JoVE (Journal Vis. Exp. (2016) e53475 %@ 1940-087X.
[10] Y. Cheng, K. Ren, C. Huang, J. Wei, Self-healing graphene oxide-based nanocomposite hydrogels serve as near-infrared light-driven valves, Sensors Actuators B Chem. 298 (2019), 126908.
[11] R. Long, C.-Y. Hui, Fracture toughness of hydrogels: measurement and interpretation, Soft Matter 12 (39) (2016) 8069–8086.
[12] J. Guo, C.-Y. Hui, M. Liu, A.T. Zehnder, The stress field near the tip of a plane stress crack in a gel consisting of chemical and physical cross-links, Proc. R. Soc. A. 475 (2019) 20180863.
[13] C.Y. Hui, J. Guo, M. Liu, A. Zehnder, Finite strain theory of a Mode III crack in a rate dependent gel consisting of chemical and physical cross-links, Int. J. Fract. 215 (1-2) (2019) 77–89.
[14] N. Bouklas, C.M. Landis, R. Huang, Effect of solvent diffusion on crack-tip fields and driving force for fracture of hydrogels, J. Appl. Mech. 82 (2015).
[15] X. Wang, W. Hong, Delayed fracture in gels, Soft Matter 8 (31) (2012) 8171, https://doi.org/10.1039/c2sm25553g.
[16] Y. Yu, C.M. Landis, R. Huang, Poroelastic effects on steady state crack growth in polymer gels under plane stress, Mech. Mater. 143 (2020) 103320 %@ 0167–6636.
[17] Y. Yu, N. Bouklas, C.M. Landis, R. Huang, Poroelastic Effects on the Time-and Rate-Dependent Fracture of Polymer Gels, J. Appl. Mech. 87 (2020).
[18] C.-Y. Hui, R. Long, J. Ning, Stress relaxation near the tip of a stationary mode I crack in a poroelastic solid, J. Appl. Mech. 80 (2013).
[19] C.-H. Yang, Y.-Y. Lin, Time-dependent fracture of mode-I cracks in poroviscoelastic media, Eur. J. Mech. 69 (2018) 78–87.
[20] Y. Yu, C.M. Landis, R. Huang, Steady-state crack growth in polymer gels: a linear poroelastic analysis, J. Mech. Phys. Solids 118 (2018) 15–39.
[21] Y. Yu, N. Bouklas, C.M. Landis, R. Huang, A Linear poroelastic analysis of time-dependent crack-tip fields in polymer gels, J. Appl. Mech. 85 (2018).

[22] Y. Li, P. Wu, H. Mazaheri, M. Xu, A linear poroelastic analysis of equilibrium asymptotic fields around stationary sharp V-notches in polymer gels, Theor. Appl. Fract. Mech. 112 (2021), 102922.
[23] W. Hong, X. Zhao, J. Zhou, Z. Suo, A theory of coupled diffusion and large deformation in polymeric gels, J. Mech, Phys, 2008 http://www.sciencedirect.com/science/article/pii/S0022509607002244 (accessed March 29, 2017).
[24] N. Bouklas, R. Huang, Swelling kinetics of polymer gels: comparison of linear and nonlinear theories, Soft Matter 8 (31) (2012) 8194, https://doi.org/10.1039/c2sm25467k.
[25] Z. Li, Z. Liu, T.Y. Ng, P. Sharma, The effect of water content on the elastic modulus and fracture energy of hydrogel, Extrem. Mech. Lett. 35 (2020), 100617.
[26] N.i. Zhang, Z. Pan, J. Lei, Z. Liu, Effects of temperature on the fracture and fatigue damage of temperature sensitive hydrogels, RSC Adv. 8 (54) (2018) 31048–31054.
[27] M.L. Williams, Stress singularities resulting from various boundary conditions in angular corners of plates in extension, J. Appl. Mech. 19 (1952) 526–8936.
[28] M.R. Ayatollahi, M. Nejati, Experimental evaluation of stress field around the sharp notches using photoelasticity, Mater. Des. 32 (2) (2011) 561–569.
[29] M.R. Ayatollahi, M. Nejati, Determination of NSIFs and coefficients of higher order terms for sharp notches using finite element method, Int. J. Mech. Sci. 53 (3) (2011) 164–177.
[30] M.R. Ayatollahi, M. Dehghany, M. Nejati, Fracture analysis of V-notched components–Effects of first non-singular stress term, Int. J. Solids Struct. 48 (10) (2011) 1579–1589.
[31] M.R. Ayatollahi, M. Dehghany, M.M. Mirsayar, A comprehensive photoelastic study for mode I sharp V-notches, Eur. J. Mech. 37 (2013) 216–230.
[32] M.M. Mirsayar, M.R.M. Aliha, A.T. Samaei, On fracture initiation angle near bi-material notches–Effects of first non-singular stress term, Eng. Fract. Mech. 119 (2014) 124–131.
[33] M.R.M. Aliha, F. Berto, A. Bahmani, S.h. Akhondi, A. Barnoush, Fracture assessment of polymethyl methacrylate using sharp notched disc bend specimens under mixed mode I+ III loading, Phys. Mesomech. 19 (4) (2016) 355–364.
[34] M. Mirsayar, B. Takabi, Fracture of underwater notched structures, Eng. Solid Mech. 4 (2016) 43–52.
[35] W. Hong, Z. Liu, Z. Suo, Inhomogeneous swelling of a gel in equilibrium with a solvent and mechanical load, Int. J. Solids Struct. 46 (17) (2009) 3282–3289, https://doi.org/10.1016/j.ijsolstr.2009.04.022.
[36] M. Dehghany, H. Saeidi Googarchin, M.R.M. Aliha, The role of first non-singular stress terms in mixed mode brittle fracture of V-notched components: an experimental study, Fatigue Fract. Eng. Mater. Struct. 40 (4) (2017) 623–641.
[37] M.R. Ayatollahi, M. Dehghany, Z. Kaveh, Computation of V-notch shape factors in four-point bend specimen for fracture tests on brittle materials, Arch. Appl. Mech. 83 (3) (2013) 345–356.
[38] A. Mousavi, M. Aliha, Determination of fracture parameters for a bi-material center cracked plate subjected to biaxial loading using FEOD method, Eng. Solid Mech. 4 (2016) 117–124.
[39] D. Systèmes, Abaqus User Subroutines Reference Guide, Version 6.14, Dassault Syst. Simulia Corp., Provid. RI, USA. (2014).
[40] Y. Mao, L. Anand, A theory for fracture of polymeric gels, J. Mech. Phys. Solids 115 (2018) 30–53.